Supporting Information for: GPS deformation related to the M_w 7.3, 2014, Papanoa earthquake (Mexico) reveals the aseismic behavior of the Guerrero seismic gap

A. Gualandi[a,1,*], H. Perfettini[2], M. Radiguet[2], N. Cotte[2], V. Kostoglodov[3]

[a] *1200 East California Boulevard, MC 100-23, Pasadena, CA 91125, USA.*

Contents of this file

- S1: Moment budget in the Guerrero gap
- S2: Files description
- Figures S1 to S10
- Tables S1 and S2

Introduction

In Section S1 we provide an estimate of the moment budget in the Guerrero gap considering the early afterslip of the 2014 Papanoa earthquake in our calculations. In Section S2 we provide the description of the ASCII files format containing the GPS position time series, the fault geometry, and the slip models. Figure S1 shows the ICA decomposition on the post-seismic data for the stations in the near-field of the 2014 Papanoa earthquake. Figure S2 shows the L-curve plots for the selection of the inversion smoothing parameter. Figure S3 shows the restitution index for the post-seismic inversion and for the co-seismic and SSE inversions. Figure S4 shows the ICA decomposition on the GPS position time series corrected for the co- and post-seismic signals. Figure S5 shows the IC number three obtained from GPS position time series corrected for the co- and post-seismic signals, and the Power Spectral Density of the temporal function associated with the IC. Figures from S6 to S12 show the detrended position time series and the fit of our model (left panels), together with the contribution of every single deformation mechanism (co-, post-seismic, and SSE, right panels). Table S1 shows the list of GPS stations used in the work and their coordinates. Table S2 shows the long-term and inter-SSE velocities at the corresponding GPS stations.

*Corresponding author
Email address: gualandi@caltech.edu (A. Gualandi)
[1]California Institute of Technology, Department of Geology and Planetary Sciences, Pasadena, CA, USA.
[2]Université Grenoble Alpes, CNRS, IRD, ISTerre, F-38000 Grenoble, France.
[3]Instituto de Geofísica, Universidad Nacional Autónoma de México, CP 04510, Ciudad de México, México.

S1. Moment budget in the Guerrero gap

It is possible that our co-seismic moment estimation is an overestimation of the real moment released by the mainshock, as described in "Discussions and Conclusions" section. UNAM (2015) and Mendoza and López (2017) studied the actual seismic waves related to the Papanoa earthquake, and thus can be considered as more reliable estimates of the actual co-seismic activity. Averaging the values found by these two groups we get:

$$M_{0\ co}^{seismic} = [9.2 \pm 0.9] \times 10^{19}\ \text{Nm} \tag{S1}$$

This means that the early post-seismic moment is the difference between our overestimation $M_{0\ co}$ and this seismic estimation:

$$M_{0\ post\ early} = M_{0\ co} - M_{0\ co}^{seismic} = [2.2 \pm 1.1] \times 10^{19}\ \text{Nm} \tag{S2}$$

We can then add to the post-seismic moment calculated from the first day after the mainshock ($M_{0\ post}$) the remaining early post-seismic moment:

$$M_{0\ post}^{total} = M_{0\ post\ early} + M_{0\ post} = [10.3 \pm 1.1] \times 10^{19}\ \text{Nm} \tag{S3}$$

In other words, using these new estimates for the co- and post-seismic moments we get that:

$$M_{0\ post}^{total} = [112 \pm 16]\%\ M_{0\ co}^{seismic} \tag{S4}$$

Assuming that the 1943 and 1979 earthquakes behaved similarly to the 2014 Papanoa earthquake by releasing $[112 \pm 16]\%$ of the co-seismic moment in post-seismic deformation, and thus:

$$M_{0\ post\ since\ 1943}^{total} = [53 \pm 5] \times 10^{19}\ \text{Nm} \tag{S5}$$

This estime must be compared with the observed moment accumulated in the 72 yr following 1943, i.e. with $M_{0\ gap\ since\ 1943} = 43.2 \times 10^{19}$ Nm. This variation from the calculations reported in Section Discussions and Conclusions, for which $M_{0\ post\ since\ 1943} = [35.0 \pm 2.8] \times 10^{19}$ Nm, gives an idea of the potential sources of uncertainty that can affect our results.

S2. Supplementary files description

For every GPS station (except OAX2 and TOL2, commercial use) we provide four different files: one containing the detrended position time series (data), and three containing the modeled co-seismic, post-seismic, and SSE displacements. The data files correspond to the black points and errorbars in Figures S6-S12 ($\pm$ a translation along the y-axis). The three modeled displacements correspond to the blue, green, and magenta lines in Figures S6-S12, respectively. Their sum gives

the cyan line in the same Figures. The name of every file corresponds to the identification name of the corresponding GPS station. Every GPS file is organized as follows:

- Column 1: Epoch (in decimal year)
- Columns 2-4: East, North, and Vertical position (in m)
- Columns 5-7: East, North, and Vertical position uncertainty (in m)

The slip evolution with time for the co-, post-seismic, and SSE slip distributions is also provided, as well as the fault geometry on which the inversions have been performed. The strike and dip slip components are presented in separate files. The number of rows is equal to the number of triangular patches in which the fault geometry has been subdivided. The post-seismic files refer to a reduced number of patches, since the inversion is limited to depths less than 45 km. The origin with respect to which the local reference frame is referring is [99.857° W, 16.822° N].

The geometry file contains 15 columns:

- Columns 1-3: x, y, and depth of the patches' center (in km)
- Columns 4-5: Strike and dip of the patches (in degrees)
- Column 6: Area of the patches (in km^2).
- Columns 7-15: x, y, and depth of the three vertices (in km)

The slip model files contain a number of columns equal to the number of epochs analyzed. The timeline is the union of all the available epochs from the GPS time series (column 1), and is also provided as a separate file (`timeline.txt`). The slip is expressed in m. The name of the files is self-explanatory:

- `co_strike_slip.txt`: co-seismic strike slip (in m)
- `co_dip_slip.txt`: co-seismic dip slip (in m)
- `post_strike_slip.txt`: post-seismic strike slip (in m)
- `post_dip_slip.txt`: post-seismic dip slip (in m)
- `SSE_strike_slip.txt`: SSE strike slip (in m)
- `SSE_dip_slip.txt`: SSE dip slip (in m)

The uncertainty on the model is not reported because it actually comprehends the full covariance matrix for every epoch. For those who are interested, we provide the temporal evolution relative to the inverted ICs (`V_post.txt`, `V_SSE_IC1.txt`, and `V_SSE_IC2.txt`), as well as the corresponding weights S (`S_post.txt`, `S_SSE_IC1.txt`, and `S_SSE_IC2.txt`), and the inverted spatial slip distributions (`L_post.txt`, `L_SSE_IC1.txt`, and `L_SSE_IC2.txt`). The files are structured as follows:

- `V_*.txt`: IC temporal function and corresponding variance (columns 1 and 2, respectively) (non-dimensional)
- `L_*.txt`: IC slip spatial distribution (column 1) (non-dimensional)

- `cov_L_*.txt`: covariance matrix of `L_*.txt`.

- `S_*.txt`: IC weights (in m).

From these matrices it is possible to reconstruct the full covariance matrix on the slip following the indications provided in Gualandi et al. (2016). For the co-seismic slip we provide the full covariance matrix relative to the offset (i.e., to the mainshock epoch): `cov_slip_co_strike_dip.txt`.

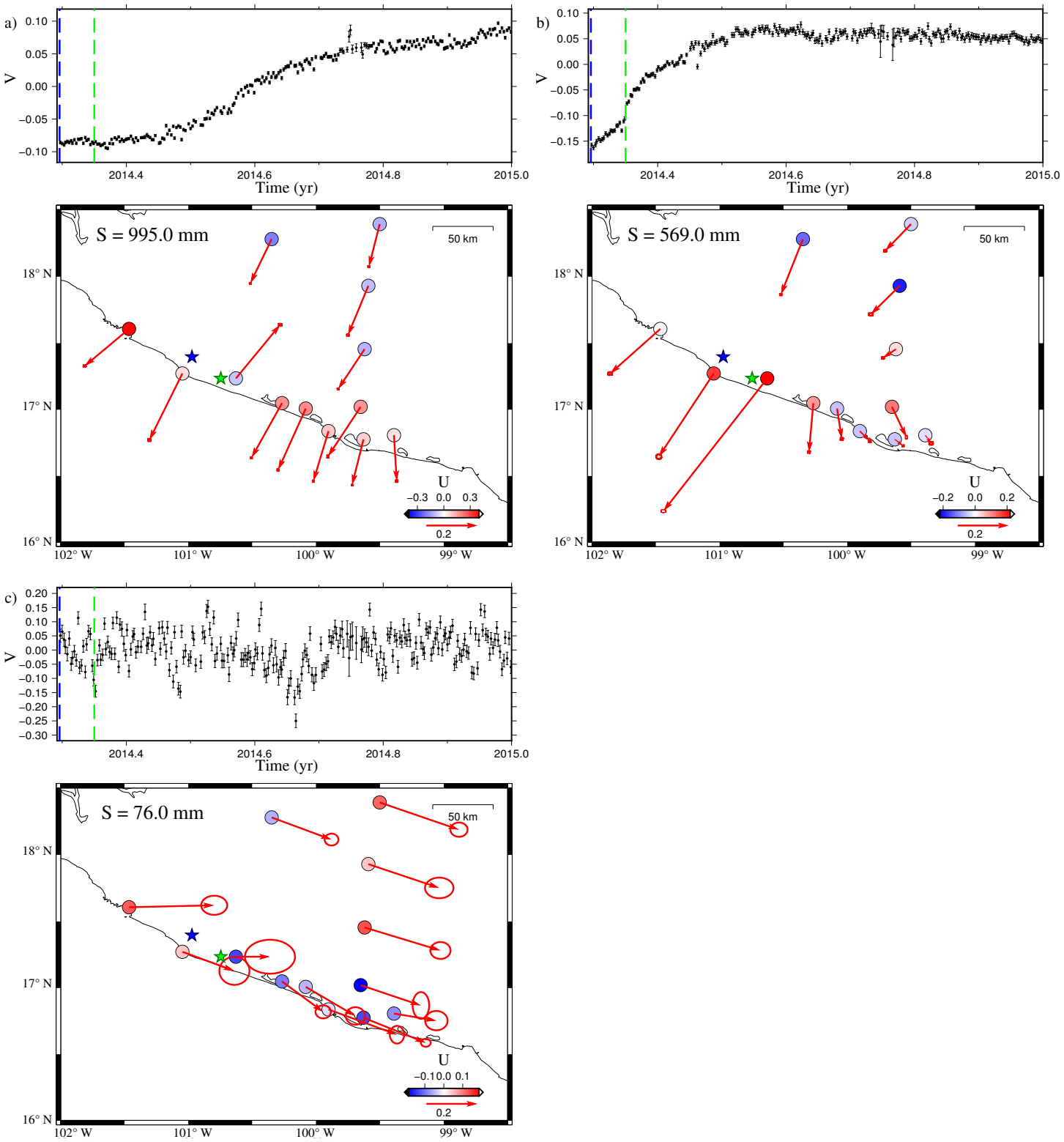

Figure S1: ICs from the analysis of the detrended time series after the mainshock, used to evaluate the post-seismic contribution. **a**), **b**), and **c**) show IC number 1, 2, and 3, respectively. Top of each panel: Temporal evolution V of the corresponding IC (black dots). Blue and green dashed lines indicate the mainshock and largest aftershock epochs. Bottom of each panel: Spatial distribution U of the corresponding IC in map view. Arrows/Dots: Horizontal/Vertical response. In the top left corner of the map also the weight S is shown. Blue and green stars indicate the mainshock and largest aftershock locations. Panel **b** is the same as Figure 2.

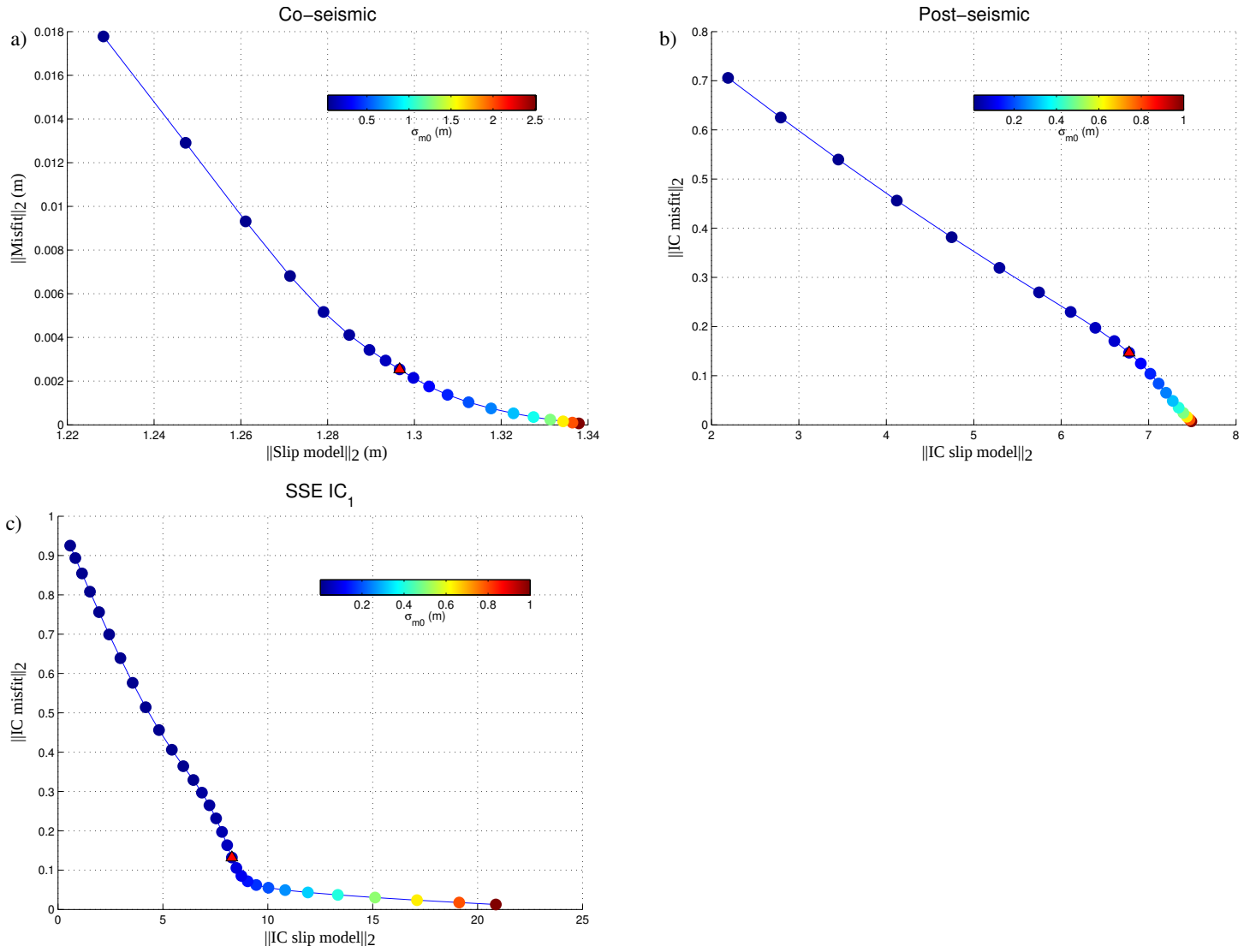

Figure S2: L-curve plots for the selection of the smoothing parameter $sigma_{m\ 0}$. The red triangle indicates the chosen value: $10^{-0.7}$ m, 10^{-1} m, and $10^{-1.2}$ m for the co-seismic, post-seismic, and SSE inversions, respectively. For the post-seismic case the curve is not actually following a typical L-shape, and we chose the indicated value in order to avoid data overfit.

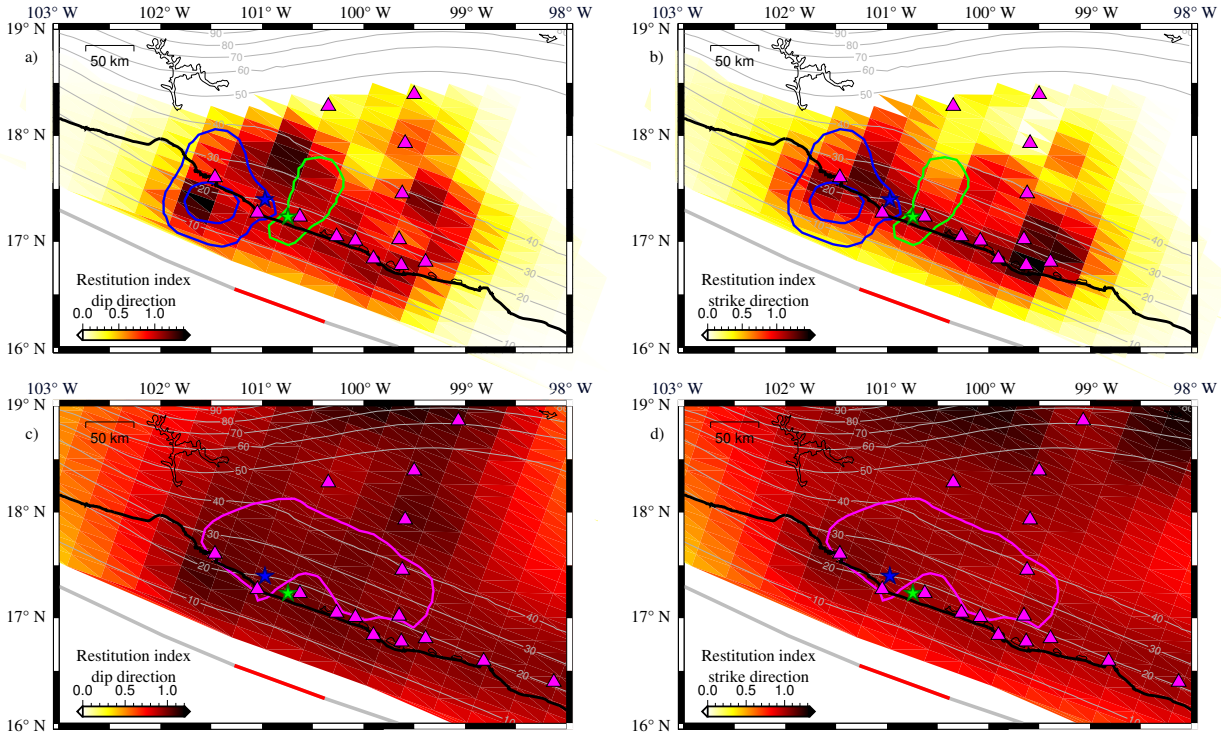

Figure S3: Restitution index, equal to the sum of the rows of the resolution matrix (see equation (3.63) of Tarantola (2005)) relative to the strike and dip directions. Low resolution areas (< 0.5) indicate not well resolved regions. Values around 1 means that the mean slip amplitude on the corresponding patch is properly retrieved. **a**) indicates the resolution index for the post-seismic inversion. **b**) as **a**), but for the SSE inversion.

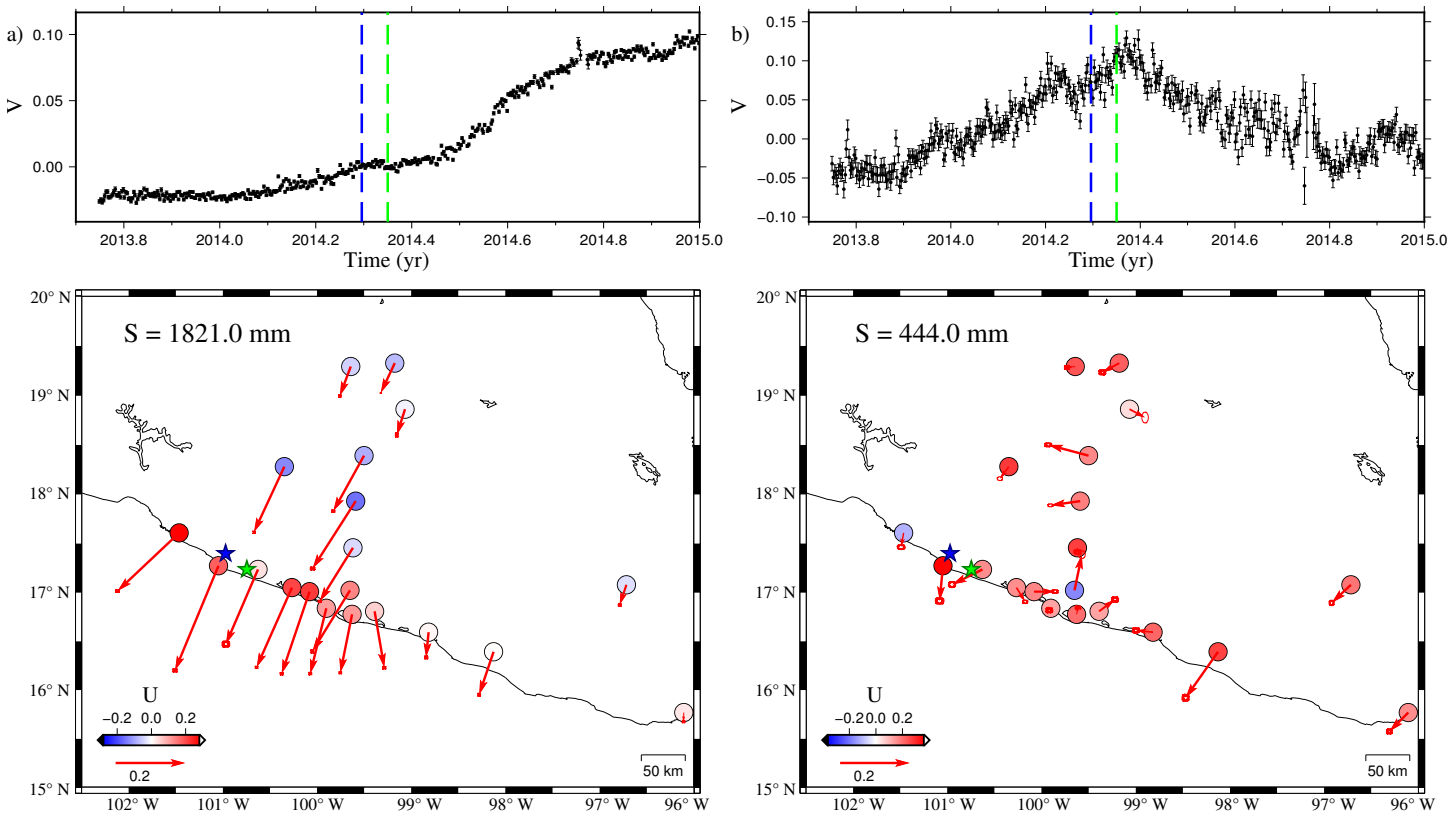

Figure S4: ICs from the analysis of the co- and post-seismic corrected position time series. **a**) and **b**) show IC number 1 and 2, respectively. Top of each panel: Temporal evolution V of the corresponding IC (black dots). Blue and green dashed lines indicate the mainshock and largest aftershock epochs. Bottom of each panel: Spatial distribution U of the corresponding IC in map view. Arrows/Dots: Horizontal/Vertical response. In the top left corner of the map also the weight S is shown. Blue and green stars indicate the mainshock and largest aftershock locations.

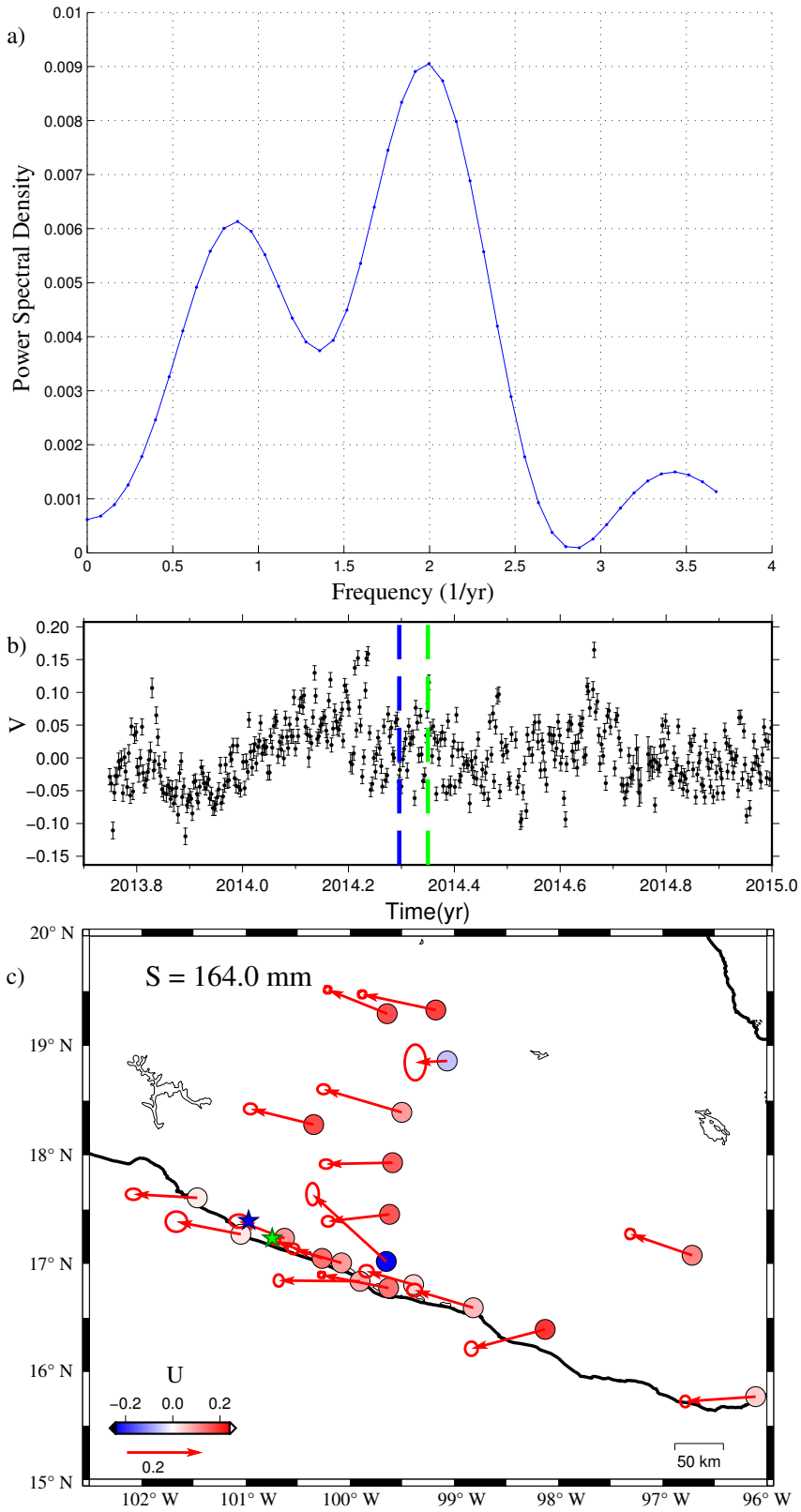

Figure S5: IC number three from the analysis of the co- and post-seismic corrected position time series. **a**) Power Sepctral Density of the temporal function shows peaks at 1 and 2 1/yr. **b**) Temporal evolution V of the third IC (black dots). Blue and green dashed lines indicate the mainshock and largest aftershock epochs. **c**)Spatial distribution U of the third IC in map view. Arrows/Dots: Horizontal/Vertical response. In the top left corner of the map also the weight S is shown. Blue and green stars indicate the mainshock and largest aftershock locations.

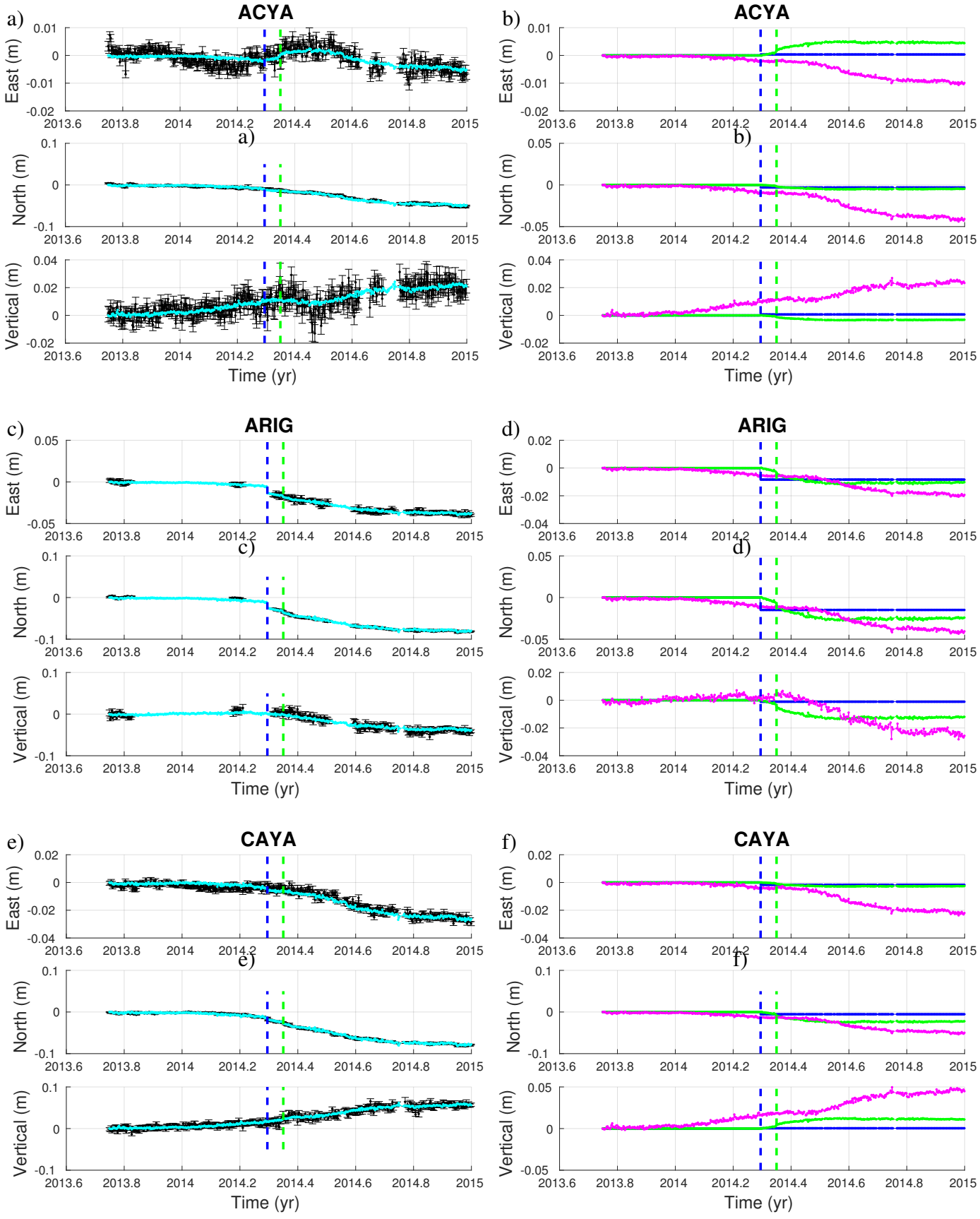

Figure S6: Left: Black: raw detrended GPS position time series. Cyan: GPS position time series reconstruction from the co- and post-seismic models and the SSE model. Right: Relative contributions to the final model. Blue/Green/Magenta: co-seismic/post-seismic/SSE displacement. In each panel, blue and green vertical lines indicate the mainshock and largest aftershock epochs, respectively.

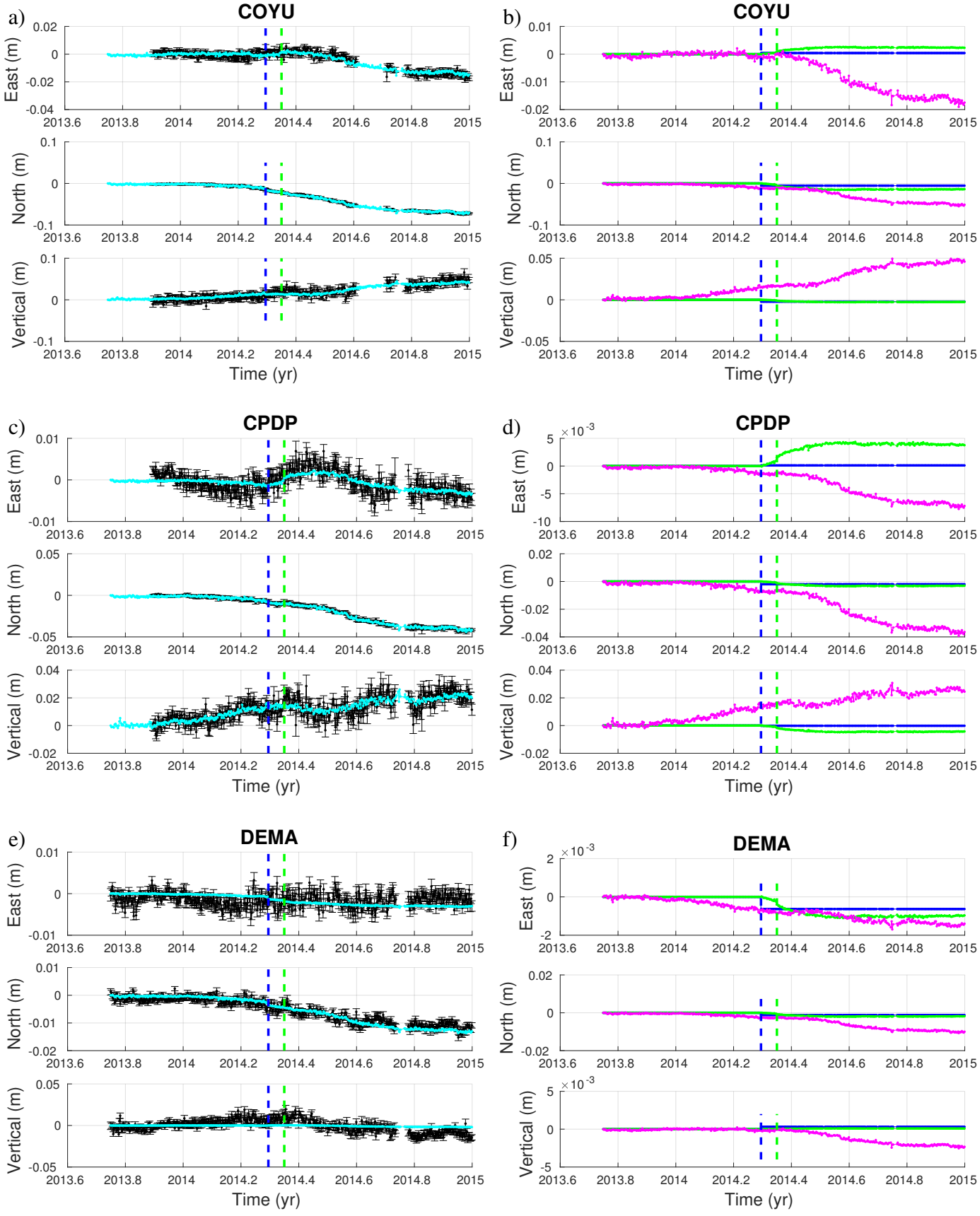

Figure S7: Left: Black: raw detrended GPS position time series. Cyan: GPS position time series reconstruction from the co- and post-seismic models and the SSE model. Right: Relative contributions to the final model. Blue/Green/Magenta: co-seismic/post-seismic/SSE displacement. In each panel, blue and green vertical lines indicate the mainshock and largest aftershock epochs, respectively.

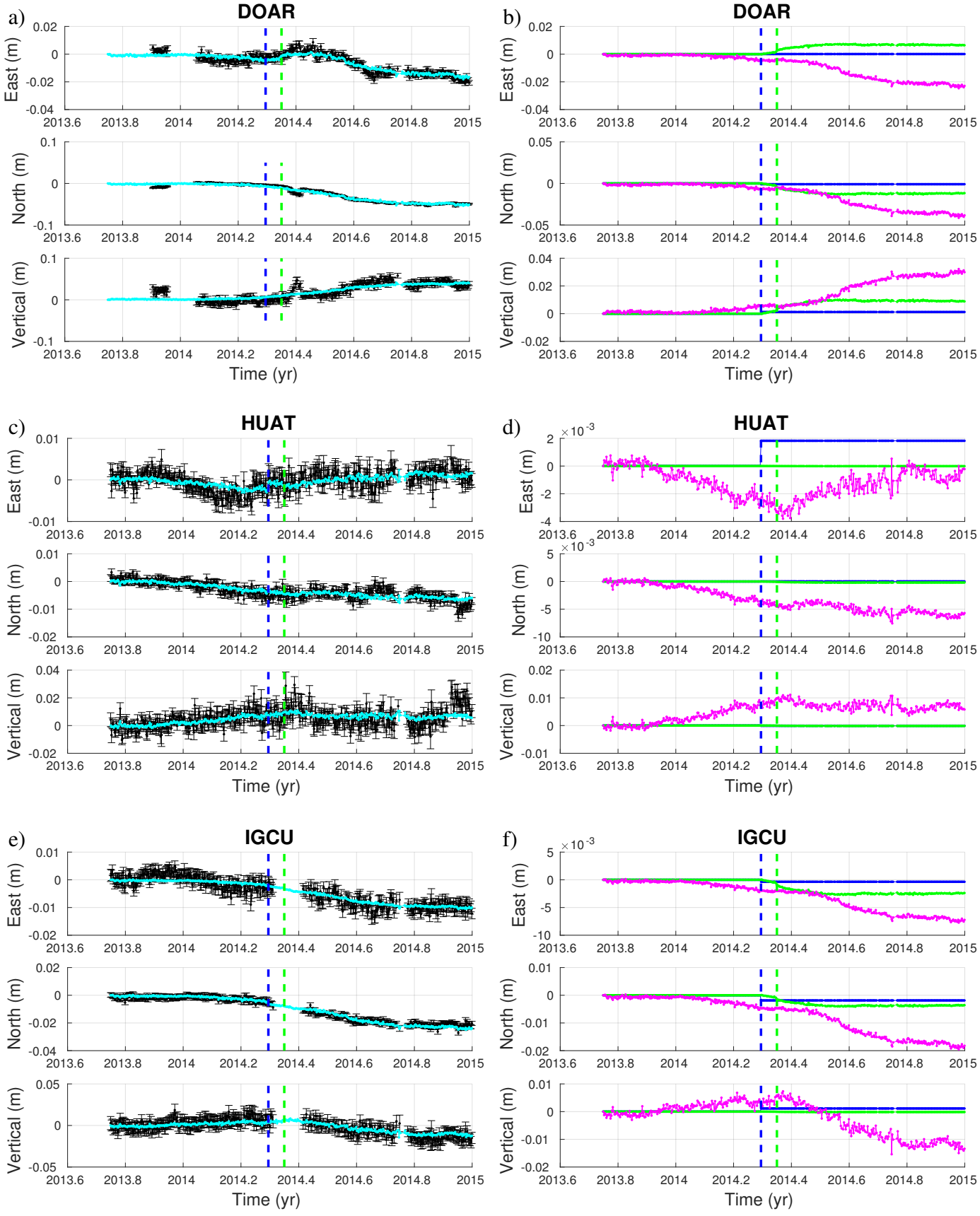

Figure S8: Left: Black: raw detrended GPS position time series. Cyan: GPS position time series reconstruction from the co- and post-seismic models and the SSE model. Right: Relative contributions to the final model. Blue/Green/Magenta: co-seismic/post-seismic/SSE displacement. In each panel, blue and green vertical lines indicate the mainshock and largest aftershock epochs, respectively.

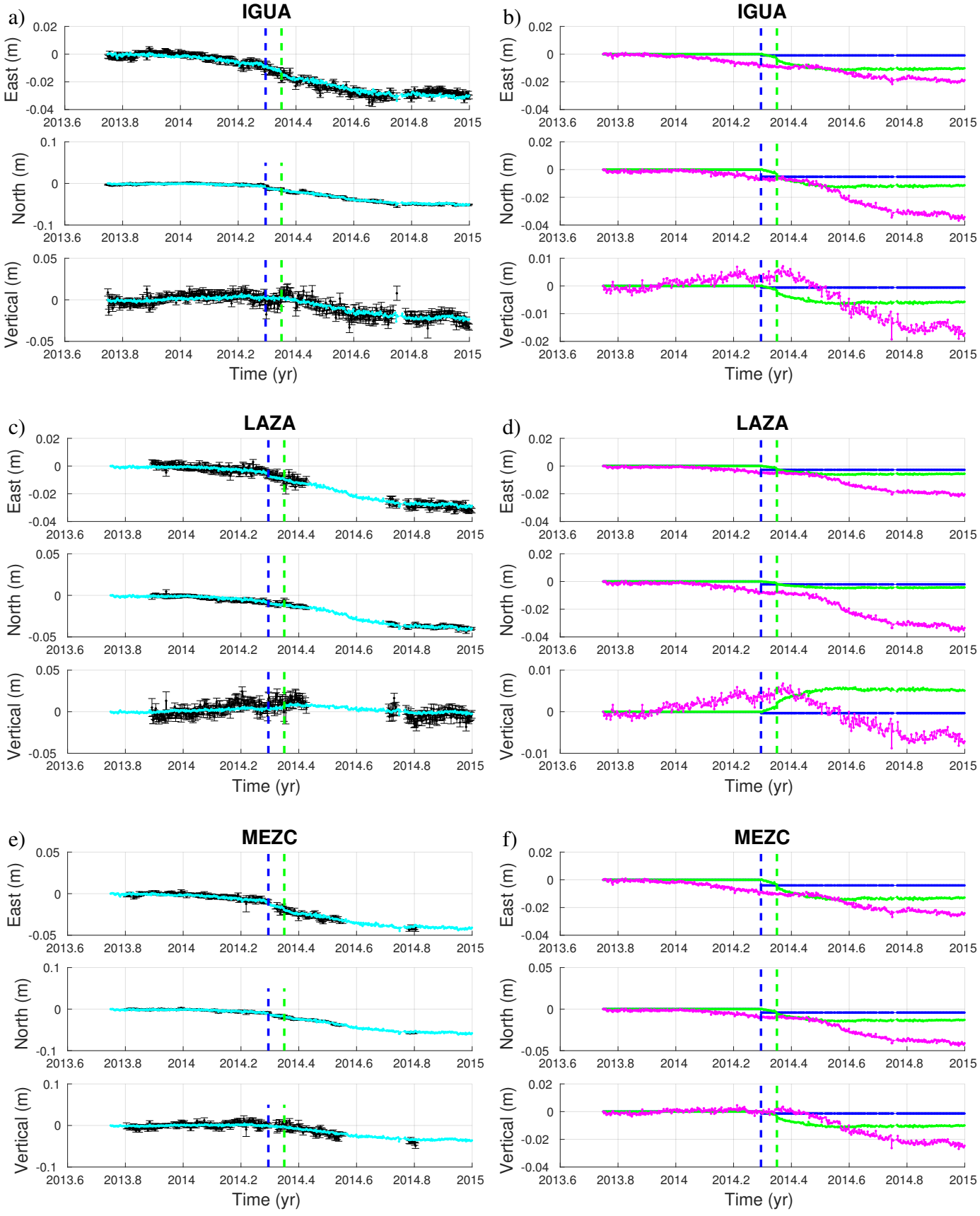

Figure S9: Left: Black: raw detrended GPS position time series. Cyan: GPS position time series reconstruction from the co- and post-seismic models and the SSE model. Right: Relative contributions to the final model. Blue/Green/Magenta: co-seismic/post-seismic/SSE displacement. In each panel, blue and green vertical lines indicate the mainshock and largest aftershock epochs, respectively.

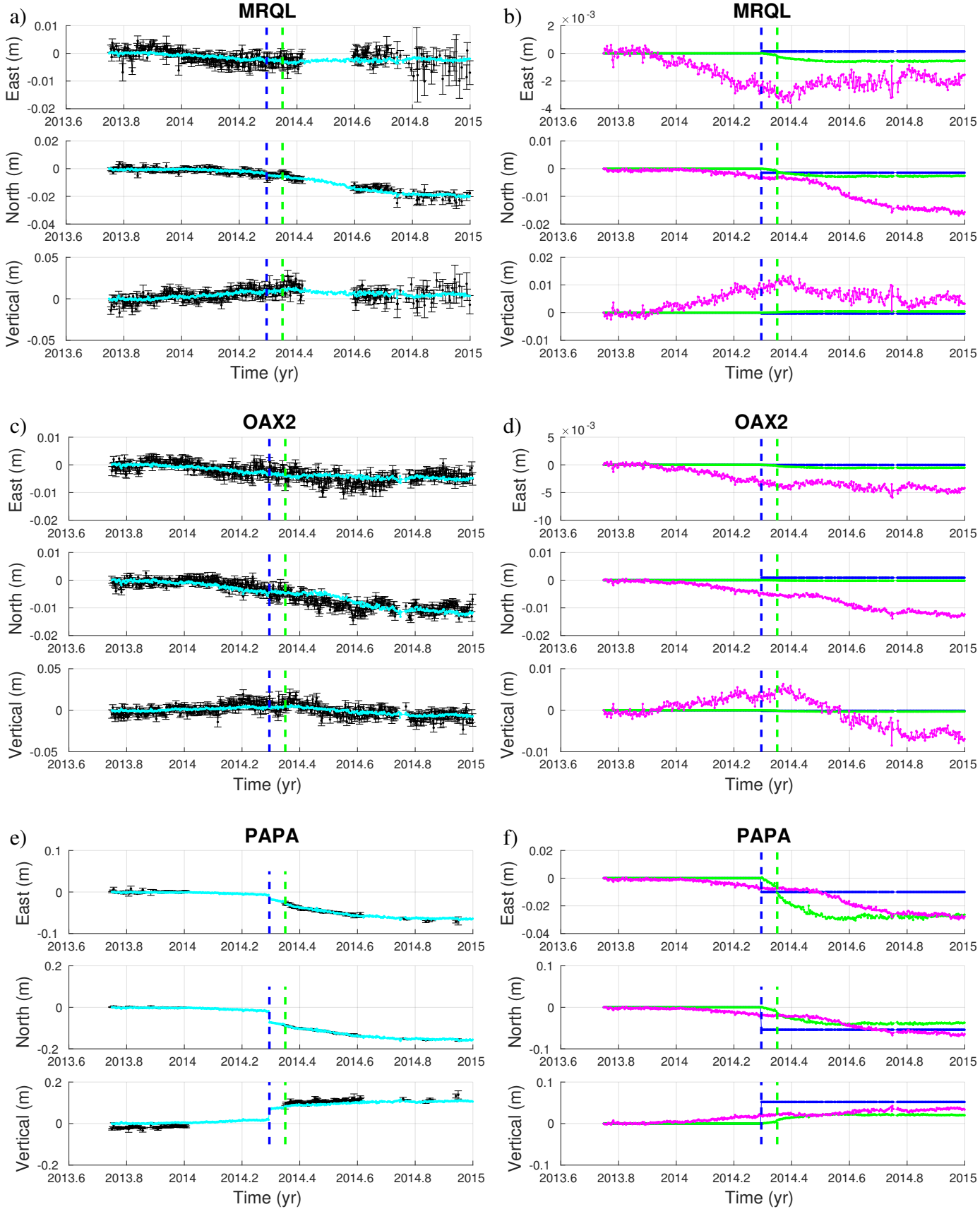

Figure S10: Left: Black: raw detrended GPS position time series. Cyan: GPS position time series reconstruction from the co- and post-seismic models and the SSE model. Right: Relative contributions to the final model. Blue/Green/Magenta: co-seismic/post-seismic/SSE displacement. In each panel, blue and green vertical lines indicate the mainshock and largest aftershock epochs, respectively.

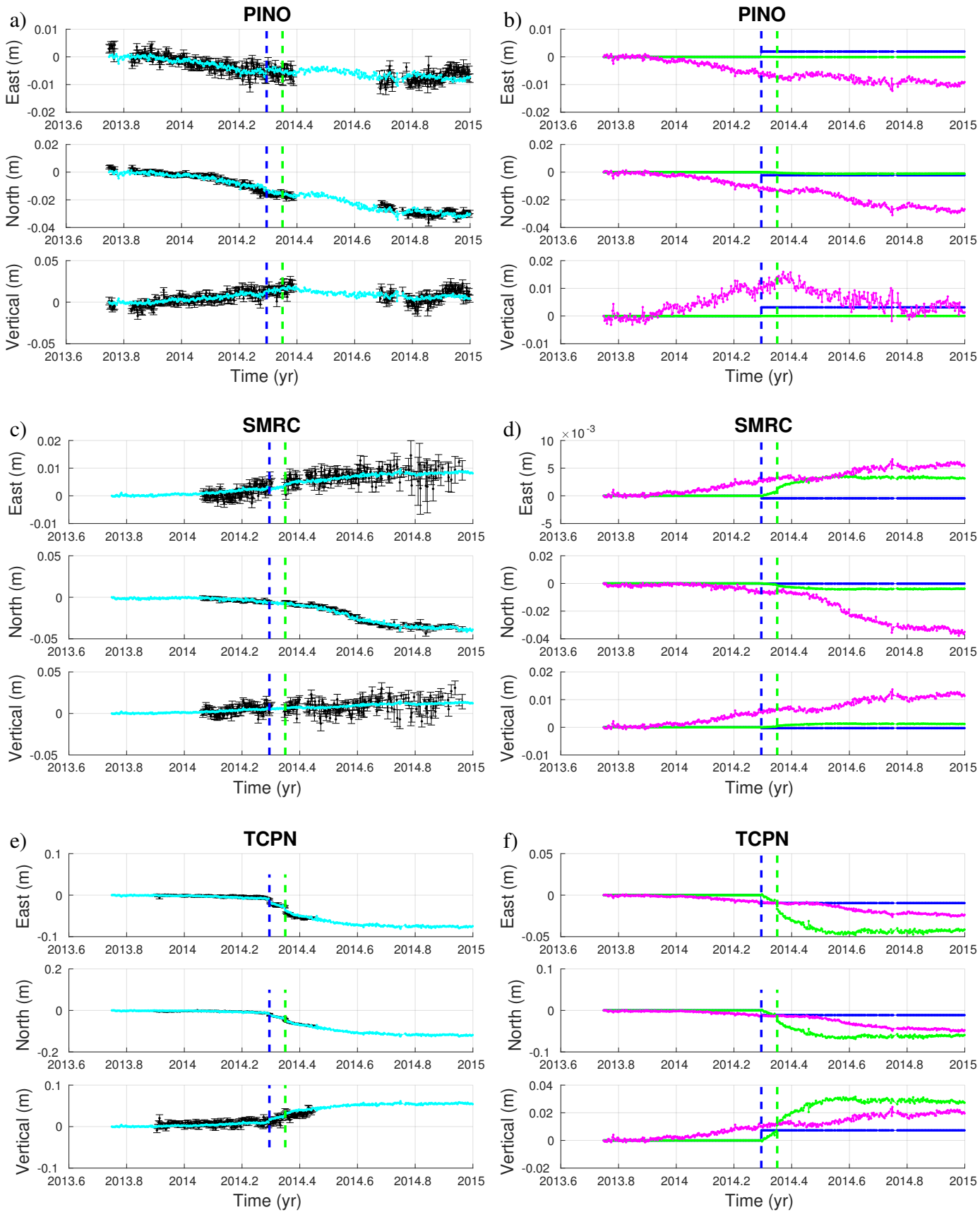

Figure S11: Left: Black: raw detrended GPS position time series. Cyan: GPS position time series reconstruction from the co- and post-seismic models and the SSE model. Right: Relative contributions to the final model. Blue/Green/Magenta: co-seismic/post-seismic/SSE displacement. In each panel, blue and green vertical lines indicate the mainshock and largest aftershock epochs, respectively.

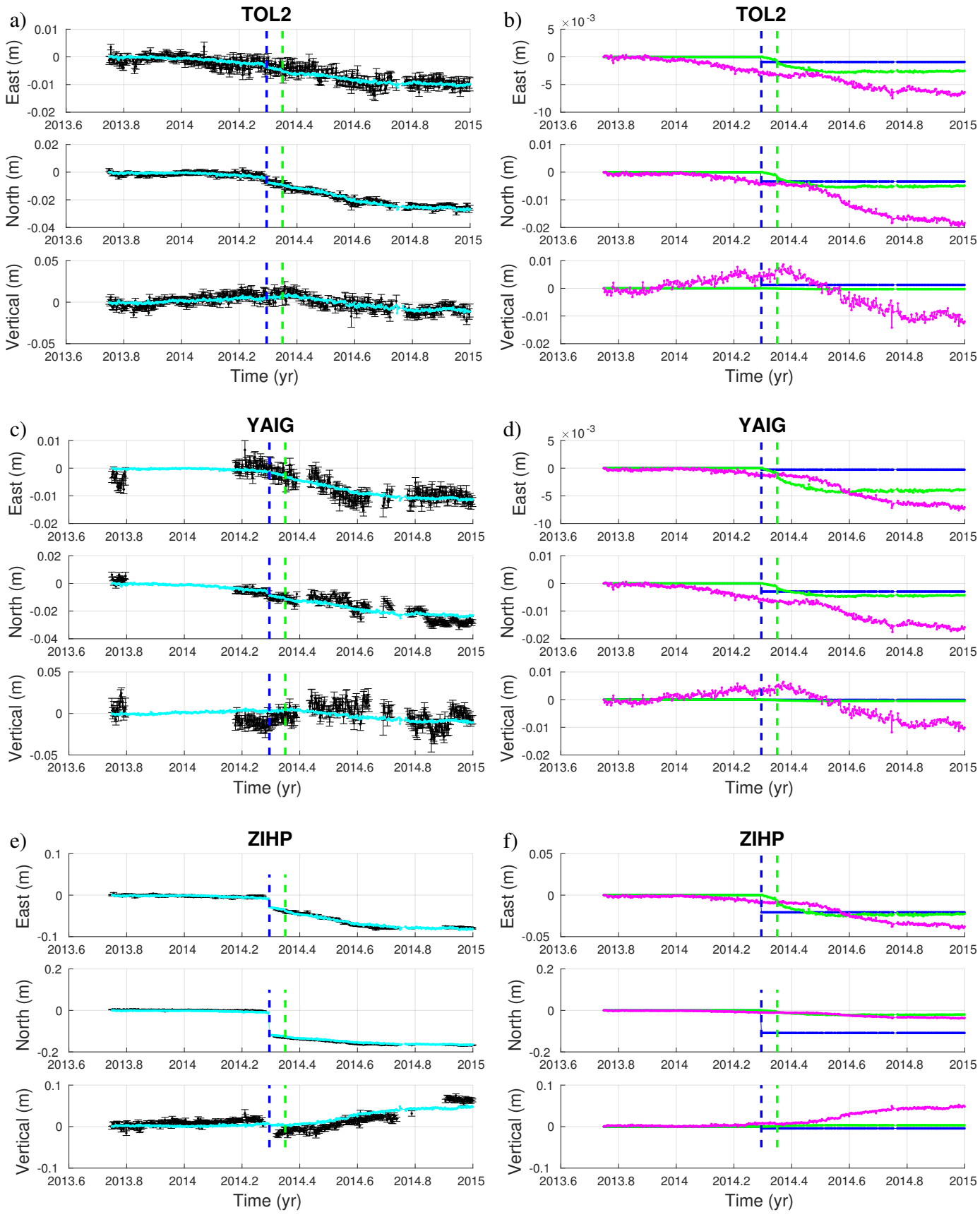

Figure S12: Left: Black: raw detrended GPS position time series. Cyan: GPS position time series reconstruction from the co- and post-seismic models and the SSE model. Right: Relative contributions to the final model. Blue/Green/Magenta: co-seismic/post-seismic/SSE displacement. In each panel, blue and green vertical lines indicate the mainshock and largest aftershock epochs, respectively.

Table S1: cGPS stations name (column 1), longitude (column 2), latitude (column 3). Symbols in last three columns indicate if the station has been used for the study of the corresponding geophysical process (Y if used, N if not used).

Station name	Longitude (°) W	Latitude (°) N	Co-seismic study	Post-seismic study	SSE study
ACYA	99.9030	16.8380	Y	Y	Y
ARIG	100.3480	18.2800	Y	Y	Y
CAYA	100.2670	17.0490	Y	Y	Y
COYU	100.0810	17.0080	Y	Y	Y
CPDP	99.6290	16.7760	Y	Y	Y
DEMA	99.0350	20.3000	Y	N	Y
DOAR	99.6510	17.0210	Y	Y	Y
HUAT	96.1080	15.7690	Y	N	Y
IGCU	99.1763	19.3266	Y	N	Y
IGUA	99.5020	18.3920	Y	Y	Y
LAZA	99.6200	17.4550	Y	Y	Y
MEZC	99.5910	17.9300	Y	Y	Y
MRQL	98.8172	16.5930	Y	N	Y
OAX2	96.7170	17.0780	Y	N	Y
PAPA	101.0470	17.2720	Y	Y	Y
PINO	98.1270	16.3930	Y	N	Y
SMRC	99.3900	16.8070	Y	Y	Y
TCPN	100.6280	17.2350	Y	Y	Y
TOL2	99.6430	19.2930	Y	N	Y
YAIG	99.0670	18.8620	Y	N	Y
ZIHP	101.4650	17.6070	Y	Y	Y

Table S2: cGPS stations name (column 1), long-term velocity (columns 2-4), inter-SSE velocity (columns 5-7). For too short time series velocities are not estimated.

Station name	v_{east} (m/yr)	v_{north} (m/yr)	$v_{vertical}$ (m/yr)	v_{east} (m/yr)	v_{north} (m/yr)	$v_{vertical}$ (m/yr)
ACYA	0.0102 ± 0.0024	0.0093 ± 0.0022	-0.008 ± 0.006	0.0123 ± 0.0024	0.0200 ± 0.0021	-0.013 ± 0.006
ARIG	-	-	-	0.0077 ± 0.0020	0.0134 ± 0.0017	0.005 ± 0.007
CAYA	0.007 ± 0.008	0.0033 ± 0.0007	-0.0019 ± 0.0020	0.0117 ± 0.0022	0.0160 ± 0.0021	-0.015 ± 0.007
COYU	0.0055 ± 0.0024	0.0076 ± 0.0022	-0.006 ± 0.006	0.0110 ± 0.0024	0.0168 ± 0.0018	-0.013 ± 0.008
CPDP	0.0094 ± 0.0020	0.0105 ± 0.0018	-0.005 ± 0.005	0.0119 ± 0.0023	0.0187 ± 0.0016	-0.014 ± 0.006
DEMA	0.0012 ± 0.0019	0.0014 ± 0.0017	-0.002 ± 0.005	0.0017 ± 0.0020	0.0015 ± 0.0016	-0.002 ± 0.006
DOAR	0.0077 ± 0.0018	0.0077 ± 0.0016	-0.001 ± 0.005	0.011 ± 0.003	0.018 ± 0.003	-0.010 ± 0.009
HUAT	-	-	-	0.012 ± 0.003	0.0166 ± 0.0027	-0.010 ± 0.006
IGCU	-	-	-	-	-	-
IGUA	0.0046 ± 0.0020	0.0031 ± 0.0018	0.001 ± 0.005	0.0073 ± 0.0020	0.0110 ± 0.0024	0.005 ± 0.006
LAZA	0.0095 ± 0.0020	0.0064 ± 0.0018	0.000 ± 0.005	0.0095 ± 0.0022	0.0135 ± 0.0018	0.000 ± 0.007
MEZC	0.0068 ± 0.0020	0.0047 ± 0.0018	0.001 ± 0.005	0.0104 ± 0.0021	0.0152 ± 0.0019	0.007 ± 0.006
MRQL	0.019 ± 0.004	0.015 ± 0.003	-0.003 ± 0.009	0.0129 ± 0.0029	0.0179 ± 0.0023	-0.002 ± 0.008
OAX2	-	-	-	0.0062 ± 0.0018	0.0107 ± 0.0022	0.003 ± 0.006
PAPA	-	-	-	0.0129 ± 0.0023	0.0136 ± 0.0020	-0.009 ± 0.007
PINO	0.0100 ± 0.0018	0.0096 ± 0.0016	-0.003 ± 0.005	0.0116 ± 0.0023	0.0152 ± 0.0022	-0.010 ± 0.007
SMRC	0.012 ± 0.003	0.0073 ± 0.0029	-0.006 ± 0.008	0.004 ± 0.003	0.0187 ± 0.0023	-0.008 ± 0.007
TCPN	-	-	-	0.0127 ± 0.0021	0.0149 ± 0.0017	-0.015 ± 0.006
TOL2	0.0018 ± 0.0029	0.0024 ± 0.0023	-0.002 ± 0.006	0.0042 ± 0.0016	0.0053 ± 0.0016	-0.000 ± 0.006
YAIG	0.0023 ± 0.0016	0.0020 ± 0.0014	-0.000 ± 0.004	0.0029 ± 0.0024	0.005 ± 0.003	-0.001 ± 0.009
ZIHP	0.0131 ± 0.0020	0.0100 ± 0.0018	0.001 ± 0.005	0.0151 ± 0.0024	0.0179 ± 0.0019	-0.004 ± 0.006

Bibliography

A. Gualandi, J. P. Avouac, J. Galetzka, J.F. Genrich, G. Blewitt, L.B. Adhikari, B.P. Koirala, R. Gupta, B.N. Upreti, B. Pratt-Sitaula, and J. Liu-Zeng. Pre- and post-seismic deformation related to the 2015, $\mathcal{M}_w$7.8 Gorkha Earthquake, Nepal. *Tectonophysics*, 2016. http://dx.doi.org/10.1016/j.tecto.2016.06.014.

C. Mendoza and M.R. Martínez López. The Mw 7.3 Papanoa, Mexico earthquake of April 18, 2014: Implications for recurrent $M > 7$ thrust earthquakes in western Guerrero. *Geofís. Int.*, 56(1):13–26, 2017. doi:10.19155/geofint.2017.056.1.2.

A. Tarantola. *Inverse Problem Theory and Methods for Model Parameter Estimation*. SIAM, 2005.

Seismology Group UNAM. Papanoa, Mexico earthquake of 18 April 2014 M_w 7.2). *Geofís. Int.*, 54:363–386, 2015.